We are IntechOpen, the world's leading publisher of Open Access books Built by scientists, for scientists

4,800
Open access books available

122,000
International authors and editors

135M
Downloads

Our authors are among the

154
Countries delivered to

TOP 1%
most cited scientists

12.2%
Contributors from top 500 universities

WEB OF SCIENCE™

Selection of our books indexed in the Book Citation Index
in Web of Science™ Core Collection (BKCI)

Interested in publishing with us?
Contact book.department@intechopen.com

Topological Methods for Singularity-Free Path-Planning

Davide Paganelli
University of Bologna
Italy

1. Introduction

Due to their multi-loop architecture, parallel manipulators can reach higher stiffness and load-bearing capability than serial manipulators of equivalent weight. This feature has made them attractive for many applications, including high-precision machining tools, space robots and high-speed manipulators. Unfortunately, the drawback of parallel architectures is the more entangled kinematics, which causes many a problem during design and operation of parallel machines.

The first problem is that it may be impossible to reach a desired configuration without disassembling the mechanism, even though such configuration satisfies all kinematic constraints. A classical trivial example is Grashof four-bar linkage (see Paul, 1979), such as the one depicted in Fig. 1. If the mechanism is at configuration 1, it is impossible to reach configuration 2 without dismantling the kinematic chain.

The configuration of a mechanism will be henceforth meant as the ordered set containing the actual poses (positions and orientations) of all the links of a mechanism. If the pose of at least one link changes, then the configuration changes.

The configuration space of a mechanism is the manifold containing all allowed configurations of the mechanism. The problem of determining whether or not any configurations can be reached is strictly connected with the number of disjoint regions composing the configuration space. If the configuration space is connected, then any configuration can be reached. On the other hand, if the configuration space is composed of two or more disjoint regions, there will always exist unreachable configurations.

Such disjoint regions were named assembly circuits for single-dof mechanism in (Chase & Mirth, 1993), where an interesting discussion is provided to discriminate circuits from branches. Many authors tackled the problem of counting the different assembly circuits in single-dof mechanisms (see for example (Chase & Mirth, 1993), (Mirth &Chase, 1993), (Midha et al., 1985)).

The denomination assembly configuration (AC henceforth) was introduced in (Foster & Cipra, 1998), to generalize the notion of assembly circuit to multi-dof mechanisms. A criterion was given in (Foster & Cipra, 1998) to determine the number of ACs composing the configuration space of any single-loop planar kinematic chain, which was proved to be at

most two. A counting method for the ACs of two-dof multi-loop mechanisms was given in (Foster & Cipra, 2002) and (Dou & Ting, 1998).
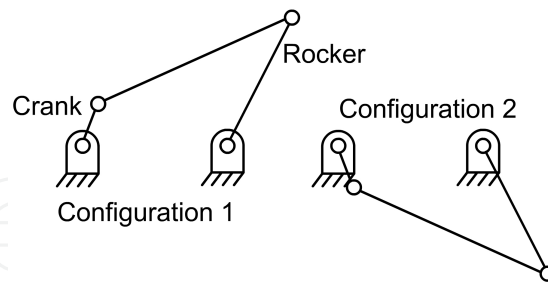
Fig. 1. A Grashof four-bar likage.

A second hindrance to path-planning toward a target configuration is the presence of singularities. In (Gosselin & Angeles, 1998) all manipulator singularities where classified into three types. Type 1 singularities occur when the inverse kinematics Jacobian matrix is singular. Such singularities are also named serial singularities, because they are typical of serial kinematic chains. Type 2 singularities occur when the direct kinematics Jacobian matrix is singular, whereas type 3 singularities occur when both the afore mentioned conditions are satisfied. Type 2 and 3 singularities are also named parallel singularities, because they are featured by parallel manipulators only.

Serial singularities might cause some loss of dexterity, but are fairly harmless, whereas parallel singularities might trigger the loss of platform control, or the structural break down of the machine. Indeed, the actuator forces required to balance the external actions on the platform might burst to infinity, while crossing a parallel singularity.

It is therefore utterly important to know whether a configuration of the manipulator can be reached or not without meeting a parallel singularity. If, at two different configurations of the manipulator, the Jacobian determinant has opposite signs, then it is impossible to go from one configuration to the other without meeting a singularity, for sooner or later the Jacobian determinant must vanish to change its sign. Nevertheless, if the sign is the same, the existence of a singularity-free path between the two configurations is uncertain.

Many solutions to the challenging problem of singularity-free path-planning are available in the literature, e.g. the geometrical methods proposed in (Dasgupta, and Mruthyunjaya, 1998), and (Bhattacharya et al., 1998), or the variational formulation adopted in (Sen et al.,2003). However, the methods hitherto proposed are mainly local, i.e., they might fail to find any singularity-free paths, though some do indeed exist.

The singularity-free path-planning problem is strictly related to the number of disjoint regions into which the configuration space is partitioned by the parallel singularity locus, i.e. the maximal connected regions free of parallel singularities. These disjoint regions will be henceforth named parallel-singularity-free regions (PSFRs). For the purpose of this paper, serial singularities will be ignored, because they are not dangerous for the manipulator.

This paper proposes a method to identify and count all the ACs and PSFRs of a fully-parallel (see Chablat & Wenger, 1998) manipulator. Once this identification process is finished, it is possible to asses whether any singularity-free path connecting any two configurations of the mechanism exists, and whether any path at all exists. The proposed method is based on some elements of differential topology, which will be recalled in the next section. The

developed method will be applied to three classes of parallel manipulators with three degrees of freedom, and numerical examples will show its effectiveness.

2. Morse Theory

Morse theory is an important branch of differential topology. Its aim is to asses the topological properties of a compact manifold through the critical points of a regular function defined on it. In this section, the main definitions and results used in the rest of the paper will be briefly recalled. Further details may be found in (Milnor, 1969).

Let M be a smooth n-dimensional compact manifold and f be a differentiable, real valued function on M. In the neighbourhood of any point P of M it is possible to define a local system of coordinates $(x_1, ... , x_n)$. With reference to these coordinates, the gradient of f at P is defined as

$$\nabla f\big|_P = \left(\frac{\partial f}{\partial x_1}\bigg|_P, ..., \frac{\partial f}{\partial x_n}\bigg|_P \right) \tag{1}$$

The points of M where $\nabla f = \mathbf{0}$ are named critical points of f. The property of being critical does not depend on the local coordinate system chosen to calculate the gradient.

The Hessian matrix of f is defined at a point P of M as

$$\mathbf{H}_f\big|_P = \left[\frac{\partial^2 f}{\partial x_i \partial x_j}\bigg|_P \right] \tag{2}$$

A critical point C of f is said to be nondegenerate if $\mathbf{H}_f\big|_C$ is nonsingular. The index λ of a nondegenerate critical point is defined as the number of negative eigenvalues of the Hessian matrix $\mathbf{H}_f\big|_C$. Neither the property of being nondegenerate nor the index depend on the local coordinate system chosen to compute $\mathbf{H}_f\big|_C$.

For each real value a, let M_a^+ be

$$M_a^+ = f^{-1}[a, +\infty) = \left\{ P \in M : f(P) \geq a \right\}, \tag{3}$$

the sub-manifold of M where the function f is greater than a. The following two relevant topological results can be stated (see (Milnor, 1969)):

Theorem 1: Let $a < b$ and suppose that the set $f^{-1}[a, b]$, consisting of all points $P \in M$ with $a \leq f(\mathrm{P}) \leq b$, contains no critical points of f. Then M_a^+ is diffeomorphic to M_b^+.
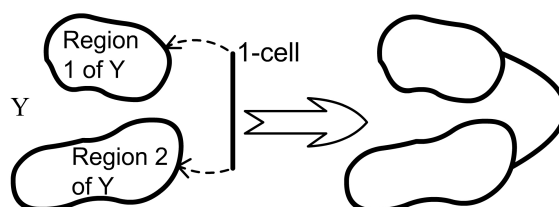

Fig. 2. Attaching a 1-cell to a topological space Y.

Theorem 2: Let c be a real value in the image of f. Suppose that $f^{-1}(c)$ contains a nondegenerate critical point of f. Then, for all sufficiently small $\varepsilon > 0$, $M_{c-\varepsilon}^{+}$ is homotopic to $M_{c+\varepsilon}^{+}$ with a k-cell attached. If λ is the index of the critical point and n the dimension of M, then k equals $n-\lambda$.

Rigorous definitions of diffeomorphism and homotopy can be found in (Hirsch, 1976) and (Whitehead, 1978). Connectedness is conserved by homotopy and diffeomorphism: if two sets are diffeomorphic or homotopic they must be composed of the same number of disjoint regions. Theorems 1 and 2 can be thus specialized in these two corollaries:

Corollary 1: Let $a<b$ and suppose that the set $f^{-1}[a,b]$ contains no critical points of f. Then the number of disjoint regions composing M_a^{+} equals the number of disjoint regions composing M_b^{+}.

Corollary 2: Let c be a real value in the image of f. Suppose that $f^{-1}(c)$ contains one nondegenerate critical point of f. Then, for all sufficiently small $\varepsilon > 0$, $M_{c-\varepsilon}^{+}$ is composed of the same number of disjoint regions as a topological space obtained by attaching a k-cell to $M_{c+\varepsilon}^{+}$. If λ is the index of the critical point and n the dimension of M, then k equals $n-\lambda$.

Corollaries 1 and 2 are useful to understand how the number of disjoint regions composing M_a^{+} varies as the real value a decreases. As long as the critical points of f contained in M_a^{+} remain the same, the number of disjoint regions is constant, by virtue of Corollary 1. As soon as a new critical point is included in M_a^{+}, the number of disjoint regions composing it may vary. By virtue of corollary 2 this variation is the same as the one obtained by attaching a k-cell to M_a^{+}.

A k-cell is the k-dimensional ball of radius 1. Roughly speaking, to attach a k-cell to a topological space Y means to glue k-cell the at its boundary to Y. Fig. 2 shows an example: a 1-cell is glued to the topological space Y. After attaching the cell, the number of disjoint regions of Y changes: it consists of one region only.

Not any variation of the number of disjoint regions composing a topological space can be obtained through the attachment of a k-cell, for the ensuing three corollaries hold (see (Paganelli, 2008)):

Corollary 3: The number of disjoint regions composing a topological space increases when a k-cell is attached to it if and only if k equals 0. In this case only one disjoint region is added.

Corollary 4: If the number of disjoint regions composing a topological space decreases when a k-cell is attached to it, then k equals 1. If a 1-cell is attached to a topological space, the number of disjoint regions composing it may remain the same or be diminished at most by one.

Corollary 5: If k is greater than 1, the number of disjoint regions composing any topological space does not change after a k-cell is attached to it.

Finally, note that corollaries 1 and 2 can be analogously formulated for the set M_a^{-}, containing all the points of M where $f \leq a$ (see (Paganelli, 2008)).

3. Analysis of Singularity Loci

In most cases, as it will be shown in section 4, the singularity locus of a manipulator is defined on the configuration space by an equation $J = 0$, where J is a Jacobian determinant. By using the notation of section 2, there is a compact manifold C, the configuration space, upon which a differentiable real-valued function J is defined. It will be assumed that the manipulator has three degrees of freedom, as the manipulators analyzed in section 4, but all results can be easily generalized for higher mobility manipulators. The aim of this section is to determine how many PSFRs where J is positive exist, i.e. how many disjoint regions compose C_a^+ according to definition (3). The same method will be applied to count the PSFRs in C_a^-, and the number of ACs composing C.
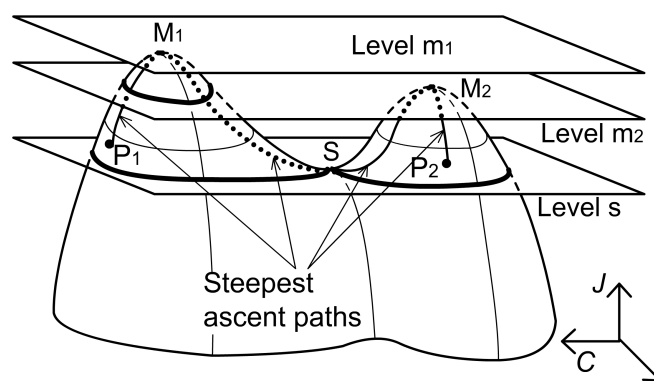

Fig. 3. Generation and joining of disjoint regions.

The evolution of the set C_a^+ is studied as the level a decreases, starting from a level above the absolute maximum, down to zero level. In order to visualize this process, pretend that the manifold C were two-dimensional, and that the graph of J could be plotted as a three-dimensional landscape on C (see Fig. 3). This fictitious lower-dimensional representation is only adopted for visualizing the real process, which occurs on a four-dimensional landscape plotted on the three-dimensional manifold C. Imagine now that the landscape is completely flooded with water. Now let the water level a decrease: as the water level reaches the height of the highest peak, M_1, an island crops out from the water. The set C_a^+ is the projection on C of the section obtained by cutting the landscape with a plane at height a. As soon as a critical point of J is met, the number of disjoint regions composing C_a^+ varies. Before meeting the absolute maximum M_1, C_a^+ was empty: it contained zero disjoint regions. After meeting the absolute maximum, the number of disjoint regions composing it changes as if a k-cell were attached to it. The maximum is a critical point of index 3 and the dimension of the manifold C is also 3, thus, k equals 0 (corollary 2). For corollary 3, if a 0-cell is attached to the set one disjoint region is added, thus, after the maximum, the number of disjoint regions is one.

The level of water a keeps on decreasing: as long as it remains between m_1 and m_2, the heights of the two maxima of Fig. 3, the number of disjoint regions remains equal to one, by virtue of corollary 1. There exists only one island above the water. As soon as maximum M_2 is reached, another island appears and a new disjoint region of C_a^+ is generated. The number of disjoint regions remains equal to two until the saddle point S is reached.

Consider a point P of C_a^+, with a contained in the open interval (s, m_2). It is possible to establish whether P belongs to the disjoint region generated by M_1 or to the disjoint region generated by M_2. The steepest ascent path starting from P must reach one of the two maxima M_1 or M_2: P belongs to the disjoint region generated by the reached maximum. Thus, the maxima work as "labels" for the disjoint regions: each disjoint region is identified by the maximum contained in it.

As the level a reaches the height of the saddlepoint S, another change of the number of disjoint regions of C_a^+ is expected. Suppose that S is a 2-saddle, i.e. the Hessian matrix has two negative eigenvalues and the index of S is equal to 2, thus the number of disjoint regions composing C_a^+ changes as if a 1-cell were attached to it. For corollary 4 the number of disjoint regions may be diminished by one or remain constant.

To decide whether or not the number of disjoint regions has decreased, it is necessary to find out to which one of the existing disjoint regions the saddle point belongs. The method to reach this goal is identical to that proposed for a noncritical point: the steepest ascent path is followed, starting from the saddle, until a maximum is reached. There are two different steepest ascent paths starting from a 2-saddle. If the steepest ascent paths reach the same maximum, then a disjoint region is joining with itself, and the number of disjoint regions remains constant. If the steepest ascent paths reach two different maxima, the disjoint regions generated by the two maxima join together (Fig. 3). To identify the disjoint region generated by the joining, the maxima inside it can be used: the steepest ascent paths starting from any points inside the new region will lead to one of its maxima.

The procedure is henceforth analogous. Each maximum generates a new disjoint region, and each 2-saddle may connect two existing disjoint regions. Following the two steepest ascent paths as for the first 2-saddle, two maxima are reached: if they belong to two different disjoint regions, such disjoint regions have joined together. If the reached maxima belong to the same disjoint region, the number of disjoint regions remains constant.

As the level a reaches the value zero, the number of disjoint regions that compose C_0^+ is determined. These disjoint regions are the PSFRs with a positive sign of the Jacobian determinant. Each PSFR is provided with a set of maxima which completely characterizes it. Furthermore, all maxima of a PSFR are connected by a network of singularity-free steepest ascent paths. Given any two configurations where the Jacobian determinant is positive (e.g. P_1 and P_2 in Fig. 3), it can be assessed whether or not they belong to the same PSFR: if the steepest ascent paths starting from the two given points reach two maxima of the same PSFR, the two points belong to the same PSFR too, otherwise not. If they do, a singularity-free path is obtained by joining the steepest ascent paths connecting the two points to the maxima and any path in the singularity-free network connecting the maxima of the PSFR.

The positive minima and the positive 1-saddles (i.e. saddle-points with index λ equal to 1) are ignored during the identification of PSFRs. In these two cases, the index λ is lesser than 2, thus only k-cells with k greater than 1 are attached to C_a^+. Corollary 5 ensures that the number of disjoint regions composing C_a^+ can neither increase nor decrease. Also any singular critical point is irrelevant to classify the PSFRs: two disjoint PSFRs may touch on the boundary at a saddle point, or a singular isolated point appears at a singular maximum, but no regions are generated or joined.

If a degenerate critical point is met, it is not possible to know whether the number of disjoint regions is changing by means of the Hessian matrix only. Higher derivatives have to be considered: the point might be a maximum, thus a new disjoint region is born. Or it might be neither a maximum nor a minimum and two or more disjoint regions could join together (see for example the "monkey-saddle" in (Milnor, 1969)).

An analogous method can be used to count and identify the number of PSFRs where the Jacobian determinant is negative, thus, at the end of this procedure, it is possible to establish to which PSFR any nonsingular point belongs.

Suppose now that the level a keeps on decreasing, below zero level. The process of generation and joining of disjoint regions continues just the same as above zero level: the negative maxima generate new disjoint regions, whereas negative 2-saddles may join existing disjoint regions, but now if the steepest ascent paths starting from negative 2-saddles reach positive maxima, they are not singularity-free anymore. However, they are still feasible paths, even though control might be lost while crossing parallel singularities.

There must exist an absolute minimum of the function J on C, for C is compact and J is continuous. As soon as level a reaches the absolute minimum level, the manifold C_a^+ coincides with the whole configuration space C. Therefore, the disjoint regions composing C_a^+ are indeed the ACs composing the whole configuration space C. As for the PSFR, each AC is endowed with a set of maxima of the function J, which completely defines it. All the maxima contained in the same AC are connected through a network of steepest ascent feasible paths.

In order to assess whether two points belong to the same AC, the steepest ascent paths starting from such points can be followed, until any of the maxima is reached. If the two maxima belong to the same AC, then there exists at least one feasible path connecting them, which can be obtained by joining the steepest ascent paths from the two points to the reached maxima, and any of the feasible paths among the network connecting the two maxima. This path is singularity-free only if the two points belong to the same PSFR, which can be assessed through the method just described.

This process can be analogously repeated for the manifold C_a^+, letting the level a increase from the absolute minimum to the absolute maximum. This second procedure is redundant for the purpose of determining the ACs, but it might be useful to find out which negative PSFRs belong to which AC, and to cross-check the results hitherto obtained.

The procedure described in the previous two sections can be summarized as follows:

1) All critical points of the Jacobian determinant J on the configuration space C are determined.

2) The critical points are classified into positive and negative maxima and into positive and negative 1- and 2-saddles.

3) The two steepest ascent paths are followed, starting from each positive 2-sadlle up to two positive maxima. The two positive maxima, and any maxima belonging to their PSFRs are assigned to the same PSFR. After all the positive 2-saddles have been processed, the positive maxima belonging to each positive PSFR are stored.

4) The two steepest ascent paths are followed, starting from each negative 2-sadlle up to two maxima. The two maxima, and any maxima belonging to their ACs are assigned to the same AC. After having processed all negative 2-saddles, the maxima of each AC are stored.

5) Step 3) is repeated, suitably modified, for the negative PSFRs, to find the negative minima contained in each negative PSFR.

6) Step 4) is repeated, suitably modified, for the positive 1-saddles, to find the minima contained in each AC.

4. Case studies

4.1 3UPS Spherical wrists

Spherical wrists are manipulators whose task is to position a rigid body with a fixed point. Thus, by moving the actuators, the orientation of the platform is varied. 3UPS spherical wrists devise a simple parallel architecture to reach this target, which is depicted in Fig. 4.

A 3UPS spherical wrist is composed of a platform, connected to the base by a spherical joint, and three legs, composed of two rigid bodies connected through a prismatic joint. The three legs are connected to the base and to the platform by means of a spherical joint and a universal joint. The universal joint could possibly be replaced by a spherical joint, but the legs would gain a passive rotational degree of freedom which might be undesired.

Let S and S' be two reference frames, attached to the base and to the platform respectively, and with the origin in the centre of the spherical joint between the platform and the base. Let the three points P_1, P_2, and P_3 be the centres of the joints between the base and the legs, and the three points Q_1, Q_2, and Q_3 be the centers of the joints between the platform and the legs. The kinematic architecture of any 3UPS wrist is identified by the three vectors $\mathbf{p}_1$, $\mathbf{p}_2$, and $\mathbf{p}_3$, containing the coordinates of points P_1, P_2, and P_3 relative to frame S, along with the three vectors $\mathbf{q}_1$, $\mathbf{q}_2$, and $\mathbf{q}_3$, containing the coordinates of points Q_1, Q_2, and Q_3 relative to frame S'.

3UPS spherical wrists were first studied in (Innocenti & Parenti-Castelli , 1993), where the direct kinematics problem was solved. In (Sefrioui & Gosselin, 1994) the singularity locus of 3UPS spherical wrists was studied, and a representation method was proposed. However, in the following sections a different parameterization and visualization will be adopted.
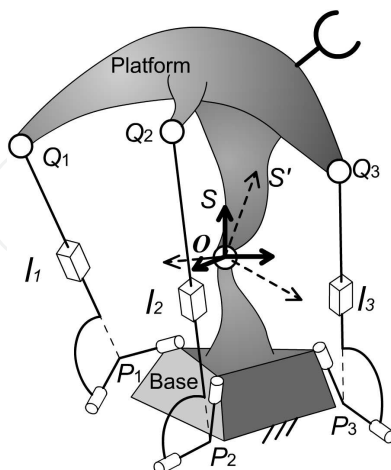

Fig. 4. 3UPS spherical wrist.

The workspace of a 3UPS spherical wrists contains all possible orientations of the platform. According to Euler theorem, any possible orientation of a rigid body with a fixed point can be obtained from a given reference position of the body by rotating of an angle θ about an

axis directed as a unit vector **u** and containing the fixed point. Therefore, adopted a reference position where frames S' and S coincide, any orientation of the platform can be defined by way of a unit vector **u** and an angle θ. The orientations of the platform associated to **u** and θ, and to - **u** and θ always coincide, thus the variation range of the angle θ can be restricted to the interval $[0, \pi]$.

A possible visualization of the workspace can be obtained by considering a ball of radius π in the three-dimensional Euclidean space. With reference to Fig. 5., every point P inside the ball represents the orientation of the platform identified by the unit vector directed as the position vector of P, and by the angle θ equal to the length of the position vector of P. Thus, every orientation of the platform with an angle θ lesser than π corresponds to only one point inside the ball, whereas any orientation with $\theta = \pi$ is identified by two diametrically opposite points on the boundary sphere of the ball.

It is useful to introduce a more homogeneous parameterization of the orientation of a rigid body, i.e. Euler parameters, which will enable an easier determination of the critical points of the Jacobian determinant. We consider the vector **e**, containing the four Euler parameters (e_0, e_1, e_2, e_3), such that:

$$e_1^2 + e_2^2 + e_3^2 + e_4^2 = 1 \tag{4}$$

and $e_0 \geq 0$. In this section, Euler parameters will be used for the mathematical representation of the workspace, whereas the visualisation of Fig. 5. will be adopted to show results on a three-dimensional graph.

Each point of the jointspace can be identified via the three length of the legs, i.e. the three distances l_i between points P_i and Q_i of Fig. 4.

The vector $(e_0, e_1, e_2, e_3, l_1, l_2, l_3)$ can be used to identify a configuration of the parallel wrist, yet, not any such vector determines an allowed configuration of the wrist, for three constraints must be satisfied. The equations expressing these constraints are derived by means of Carnot theorem applied to the three triangles P_iOQ_i, as shown in Fig. 6. For each of such triangles one can write the constraint:

$$l_i^2 = \mathbf{p}_i^T \mathbf{R} \, \mathbf{q}_i \tag{5}$$

where **R** is the rotation matrix ruling the coordinate change from S' to S, whereas $\mathbf{p}_i$ and $\mathbf{Rq}_i$ are the column vectors containing the coordinates of points P_i and Q_i in the fixed frame S.

The rotation matrix can be written as a quadratic function of the four Euler parameters, , thus Eq. (5) represents a set of three quadratic equations in Euler parameters and leg lengths. If only positive leg lengths are accepted, which indeed does not exclude any configuration of the wrist, there is only one set of leg lengths for any orientation of the platform. Thus, the workspace alone can be used to represent the whole configuration space of the wrist, and there is only one AC.
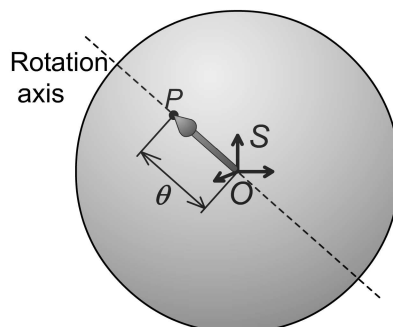
Fig. 5. Workspace of a 3UPS wrist.

In order to determine the singularity locus of the 3UPS spherical wrist, Eq. (5) is differentiated, obtaining the ensuing relationship between the virtual displacement of the platform and the virtual variations of leg lengths:

$$
\mathbf{A}\begin{pmatrix} \delta l_1 \\ \delta l_2 \\ \delta l_3 \end{pmatrix} = \mathbf{B}\begin{pmatrix} \delta e_0 \\ \delta e_1 \\ \delta e_2 \\ \delta e_3 \end{pmatrix}
\tag{6}
$$

where $\mathbf{A}$ and $\mathbf{B}$ are the Jacobian matrices of Eq. (5) with respect to leg lengths and Euler parameters respectively.

Moreover, not any virtual variation of Euler parameters is allowed, for Eq.(4) must hold for first order variations too. Thus, differentiation of Eq.(4) yields the ensuing constraint upon the virtual variations of Euler parameters:

$$
e_0 \delta e_0 + e_1 \delta e_1 + e_2 \delta e_2 + e_3 \delta e_3 = 0
\tag{7}
$$

If equations (7) and (6) are put together, the ensuing relation is obtained:

$$
\begin{pmatrix} \mathbf{A} \\ 0 \quad 0 \quad 0 \end{pmatrix}\begin{pmatrix} \delta l_1 \\ \delta l_2 \\ \delta l_3 \end{pmatrix} = \begin{pmatrix} \mathbf{B} \\ e_0 \quad e_1 \quad e_2 \quad e_3 \end{pmatrix}\begin{pmatrix} \delta e_0 \\ \delta e_1 \\ \delta e_2 \\ \delta e_3 \end{pmatrix}
\tag{8}
$$

Parallel singularities occur whenever a nonzero virtual displacement of the platform is allowed by the constraints, although the actuators undergo no virtual displacements.

This implies that the determinant of the matrix at the right-hand side of Eq. (8) vanishes. Thus the parallel singularity locus is defined as the zero level set of a function J on the configuration space, which contains all possible orientations of the platform. The function J can be obtained as:

$$
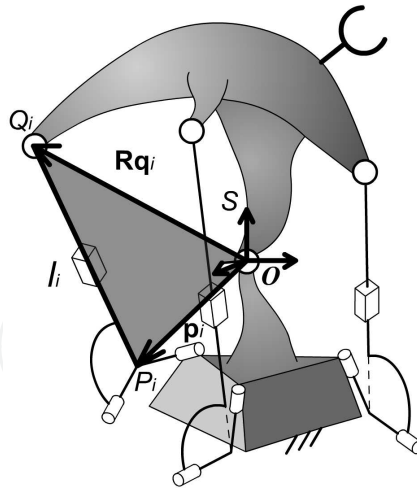J = \det\begin{pmatrix} \mathbf{B} \\ e_0 \quad e_1 \quad e_2 \quad e_3 \end{pmatrix}
\tag{9}
$$

Fig. 6. Constraints of the spherical wrist through Carnot theorem

Each element of matrix **B** is linear and homogeneous in the four Euler parameters, therefore J is a fourth-order homogeneous polynomial in the four Euler parameters. The singularity locus $J = 0$ can be represented as a two-dimensional surface cutting the workspace, and the method developed in Section 3 can be used to determine how many PSFRs are partitioned by the singularity locus, and to find out whether it is possible or not to reach a desired position in the workspace without crossing a parallel singularity.

The toughest and most important task is the determination of all critical points of the function J on the configuration space, which coincides in this case with the workspace. For the case at hand, a redundant parameterization is used, because the four Euler parameters, tied by Eq.(4) identify a point of the three dimensional manifold containing all possible orientations of a rigid body.

The most straightforward way to tackle the problem is to resort to Lagrange's multipliers. At the critical points of J, the gradient of J is parallel to the gradient of the constraint, formalized by Eq.(4), i.e.:

$$\frac{\partial J}{\partial \mathbf{e}} = \lambda \mathbf{e} \tag{10}$$

where λ is a Lagrange multiplier, and can be easily eliminated considering the ensuing equation set:

$$\begin{aligned}
(\partial J / \partial e_1) e_0 - (\partial J / \partial e_0) e_1 &= 0 \\
(\partial J / \partial e_2) e_0 - (\partial J / \partial e_0) e_2 &= 0 \\
(\partial J / \partial e_3) e_1 - (\partial J / \partial e_1) e_3 &= 0
\end{aligned} \tag{11}$$

which stems from Eq. (10) by multiplying the ith equation by e_j and by subtracting the result from the product of the jth equation by e_j, with a proper choice of i and j.

Eq.(11) is set of three homogeneous fourth-order polynomial equations, in the four Euler parameters. Each solution in the projective space of such equation, when properly normalized, is a set of Euler parameters defining a critical point of J on the workspace, except some extraneous solutions introduced while passing from Eq. (10) to Eq.(11). Such

extraneous solutions are obtained when e_0 or e_1 are posed equal to zero. If $e_0 = 0$, Eq.(11) becomes:

$$
\begin{aligned}
\left(\partial J / \partial e_0\right) &= 0 \\
\left(\partial J / \partial e_0\right) &= 0 \\
\left(\partial J / \partial e_3\right) e_1 - \left(\partial J / \partial e_1\right) e_3 &= 0
\end{aligned}
\tag{12}
$$

where the first two equations degenerate into the same one. Therefore, Eq.(12) is a set of two homogeneous equations, the first of degree three and the second of degree four, in three unknowns. By virtue of Bezout theorem, Eq.(12) admits 12 solutions, which are extraneous solutions to Eq. (10), that does not admit, in general, solutions with $e_0 = 0$.

Analogously, if $e_1 = 0$ Eq.(11) degenerates again into two equations, that yield twelve additional extraneous solutions. Eq.(11) is a set of three homogeneous equations of degree 4, therefore, by virtue of Bezout theorem, it admits $4^3 = 64$ solutions in the complex projective space. Since 24 solutions are extraneous for Eq. (10), there are 40 solutions to Eq.(11), and the real ones are critical points of J.

Such forty solutions can be obtained by partial homogenization. First of all, Eq.(11) is transformed into a non homogeneous system of equations, by posing $e_0 = 1$. In this way, any homogeneous solution with $e_0 = 0$ becomes a solution at infinity, included 12 of the 24 extraneous solutions. Then, Eq.(11) is partially homogenized, by posing $e_2 = x_1 / x_0$ and $e_3 = x_2 / x_0$, and by simplifying the denominators. In this way, Eq.(11) becomes a system of three homogeneous equations of degree four in the three variables x_1, x_2, and x_0, where variable e_1, that has been left out of partial homogenization, is hidden in the coefficients. Variables x_1, x_2, and x_0 can be got rid of by means of classical elimination methods, (see for example (Salmon, 1885)), obtaining a polynomial in the hidden variable e_1.

Stemming from a homogeneous equation set that should have 64 solutions, the resultant polynomial should be of degree 64. However, since the homogeneous equation set always possesses 12 solutions with $e_0 = 0$, the resultant polynomial must have at least 12 solutions at infinity, and its degree will be at most 52.

Furthermore, since there are always twelve extraneous solutions with $e_1 = 0$, the resultant polynomial will be divisible by the monomial e_1^{12}. By dividing the resultant by e_1^{12}, a final equation of degree 40 is obtained, that is completely purged from extraneous solutions.

The polynomial of degree 40 is solved numerically, and the values of e_2 and e_3 corresponding to each solution in e_1 are easily found (Salmon, 1885). The values obtained are homogeneous solutions with $e_0 = 1$. In order to obtain the four Euler parameters identifying the orientation of the rigid body, the four values just obtained must be normalized, so that Eq.(4) is satisfied. Should there be any critical point with $e_0 = 0$, this would be another solution at infinity to the resultant polynomial, whose degree would be lesser than 40. In this case, the loss of a solution is easily detected by the loss of one degree of the final polynomial, and the lost solution can easily be found by substituting $e_0 = 0$ into Eq. (10).

In this way, all 40 complex solutions to Eq. (10) are found, and the real ones are the critical points of the function J. These critical points must be classified into maxima, minima, 1-saddles and 2-saddles. In order to perform the classification, a local coordinate system could be chosen, and the Hessian matrix could be calculated and analyzed. However, this is not the most straightforward way to proceed, for the parameterization used henceforth is redundant, and represents no local coordinate system. At the same way Lagrange multipliers enable determination of critical points with no need of local coordinate systems, it is possible to intrinsically analyze second order variations of J in the neighborhood of a critical point through the following eigenvalue problem (see (Fletcher, 1987)):

$$\left(\mathbf{H}\big|_{\tilde{e}}^{*} - \alpha \mathbf{I}^{*} \right) \mathbf{a}^{*} = 0 \tag{13}$$

where:

- $\mathbf{H}\big|_{\tilde{e}}^{*}$ is the bordered Hessian, i.e. the Hessian matrix of the Lagrangian function, calculated at the critical point $\tilde{\mathbf{e}}$. The Lagrangian function is defined as $L(\mathbf{e}, \lambda) = J(\mathbf{e}) - \lambda \cdot c(\mathbf{e})$, where $c(\mathbf{e}) = \mathbf{e}^{T}\mathbf{e} - 1$ is the optimization constraint.

- $\mathbf{I}^{*}$ is equal to the 5x5 identity matrix, save the fifth element of the fifth row, which is equal to zero.

- $\mathbf{a}^{*}$ is a five-dimensional vector obtained appending a dummy variable to a four dimensional vector, representing a small variation of Euler parameters in the neighbourhood of the critical point.

The steepest increase or decrease directions are the directions for which the ensuing condition is satisfied:

$$\det\left(\mathbf{H}\big|_{\tilde{e}}^{*} - \alpha \mathbf{I}^{*} \right) = 0 \tag{14}$$

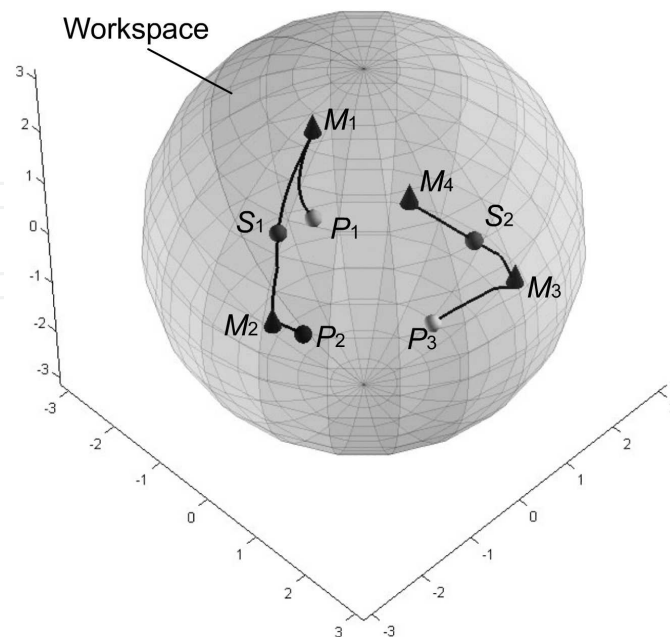Fig. 7. Critical points in the workspace of W_1

Eq.(14) is always a third order polynomial in the eigenvalue α, therefore three solutions are expected. For each solution, Eq.(13) yields the corresponding direction of steepest variation of J: it is represented by the first four components of the eigenvector $\mathbf{a}^*$ of each eigenvalue α. The eigenvectors corresponding to positive eigenvalues are steepest increase directions, whereas the eigenvectors corresponding to negative eigenvalues are steepest descent directions. The index of the critical point is thus the number of negative solutions to Eq.(14), which enables the classification of any possible critical point of J.

Also the generation of the steepest ascent or descent paths does not require the use of a local coordinate system. A small displacement in the steepest ascent direction just found is used to leave a saddle point. Then, small displacements following the projection of the gradient of J along the constraint surface described by Eq.(4) will build the steepest variation path, ending upon a maximum or a minimum. Whenever, while following a steepest ascent or descent path, a set of Euler parameters $\mathbf{e}$ with $e_0 < 0$ is reached, it is immediately replaced with $-\mathbf{e}$, which is the same position of the platform, in order that e_0 is always greater than zero, as discussed above.

The 3UPS spherical wrist W_1 will be used as a numerical application. The parameters defining manipulator W_1 are reported in Table 1.

$\mathbf{p}_1$	$\mathbf{p}_2$	$\mathbf{p}_3$	$\mathbf{q}_1$	$\mathbf{q}_2$	$\mathbf{q}_3$
(1,0,0)	(0,1,0)	(0,1,1)	(-9,2,6)/11	(6,6,7)/11	(-1,1,0)

Table 1. Parameters defining manipulator W_1

Through the elimination method just described, 32 critical points are determined, among which there are 4 positive maxima, 2 positive 2-saddles, 4 negative minima, 12 negative 1-saddles, and 10 singular 2-saddles.
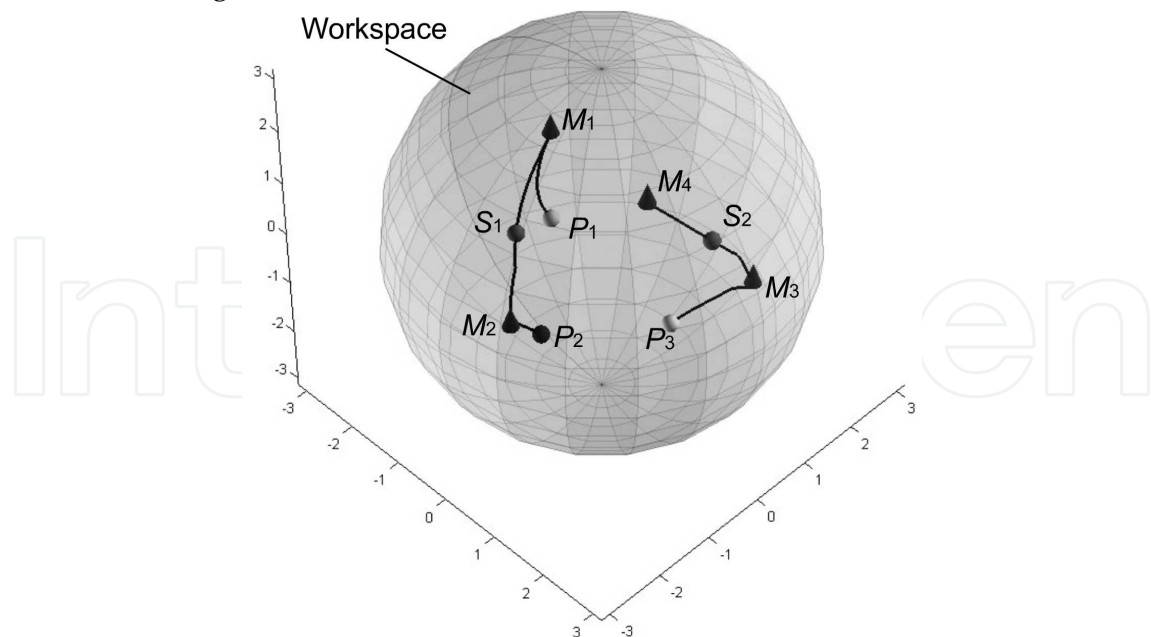

Fig. 7 shows the workspace of the spherical wrist, through the representation proposed in Fig. 5. The four positive maxima M_1, M_2, M_3 and M_4, are depicted as cones, and the two positive 2-saddles S_1 and S_2, depicted as spheres.

The steepest ascent paths starting from the two 2-saddles S_1 and S_2 join M_1 to M_2 and M_3 to M_4 respectively, thus there are two positive PSFRs. The steepest ascent paths are represented in
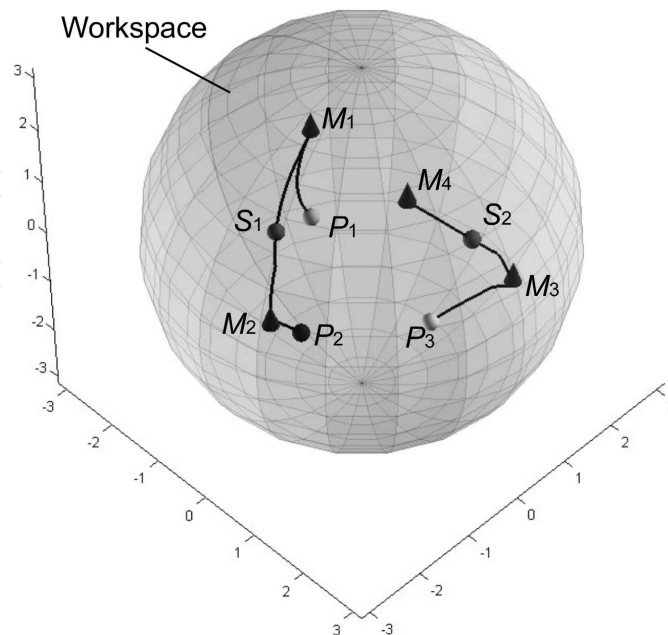

Fig. 7 as black lines.

Given the three points P_1, P_2, and P_3, where J is positive, it can be assessed to which one of the two positive regions they do belong by following the steepest ascent paths (black lines in
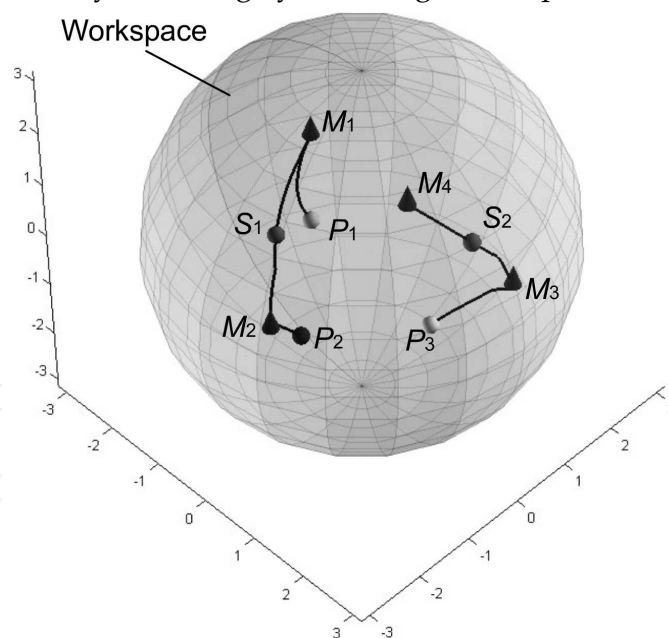

Fig. 7. The steepest ascent paths starting from P_1, P_2, and P_3 reach the maxima M_1, M_2 and M_3, respectively. Therefore P_1 and P_2 belong to the same region, and the path P_1 -M_1 -S_1 -M_2 -P_2, connecting P_1 to P_2 is singularity-free. The steepest ascent path starting from P_3 reaches M_3, which belongs to a different region, therefore there exists no singularity-free path at all to reach P_1 or P_2 starting from P_3.
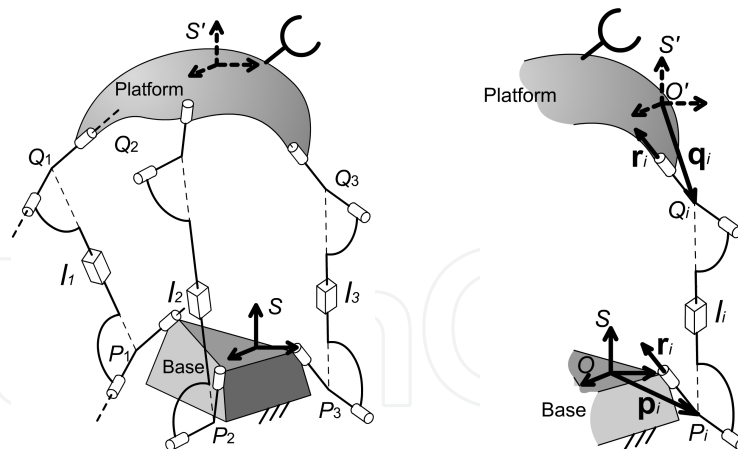
Fig. 8. Kinematic architecture of a 3UPU translational manipulator.

The four minima are all connected through a network of steepest descent paths starting from the negative saddles, therefore there is only one negative singularity-free region.

4.2 3UPU Translational Manipulators

3UPU translational manipulators have been proposed and analyzed in (Tsai, 1996), (Di Gregorio & Parenti Castelli, 1998), and (Parenti Castelli et al.., 1998).

The architecture that will be hereafter considered is that proposed in (Di Gregorio & Parenti Castelli, 1998), and sketched in Fig. 8. The platform is connected to the base by means of three legs, consisting of two links connected to each other by a prismatic joint and to the base and the platform through universal joints. The universal joints satisfy the ensuing two geometrical requirements:

- in each leg, the axes of the two revolute joints connected to the base and to the platform are parallel;
- in each leg, the axes of the two middle revolute joints, not connected to the base nor to the platform, are parallel.

It can be proved that this architecture constrains the platform to pure translational motions (see (Di Gregorio & Parenti Castelli, 1998)).

With reference to Fig. 8, the geometry of 3UPU translational manipulators, can be parametrized in the ensuing way:

- two reference frames S and S' with parallel axes, attached to the base and to the platform respectively, are defined;
- on the ith leg, the center P_i of the universal joint attached to the base is identified through its coordinate vector $\mathbf{p}_i$ in frame S;
- on the ith leg, the center Q_i of the universal joint attached to the platform is identified through its coordinate vector $\mathbf{q}_i$ in frame S';
- on the ith leg, the common directions of the axes of the revolute joints attached to the base or to the platform is identified by way of a unit vector $\mathbf{r}_i$

Therefore, the nine vectors $\mathbf{p}_i$, $\mathbf{q}_i$, and $\mathbf{r}_i$, for i=1,2,3, completely define the kinematic architecture of 3UPU translational manipulators.

The workspace of a 3UPU translational manipulator is the manifold containing all possible positions of the platform. Each point of the workspace can be identified by means of the

coordinate vector $\mathbf{x} = (x, y, z)$ of a point, for example the origin O' of S', with respect to the fixed frame S. Therefore the workspace is the whole three dimensional Euclidean space.

Any point of the jointspace is defined by the vector $\mathbf{l} = (l_1, l_2, l_3)$, containing the lengths of the three actuated legs, thus the jointspace is a subset of the three dimensional Euclidean space, too. More specifically, the length l_i is equal to the distance between points P_i and Q_i. No limits will be considered for leg length, thus each l_i can range from zero to infinity.

The vector (l_1, l_2, l_3, x, y, z) identifies a configuration of the manipulator only if the ensuing constraints are satisfied:

$$l_i^2 = (Q_i - P_i)^2 = (\mathbf{q}_i + \mathbf{x} - \mathbf{p}_i)^2 \tag{15}$$

Like the spherical wrists, if only positive lengths are accepted to describe the length of the legs, there exists only one point of the jointspace that defines a configuration along with a given point in the workspace, which means that the workspace and the configuration space can be considered as the same manifold. In other words, the vector (x,y,z) identifies both a position of the platform and a configuration of the manipulator, and there is only one AC.

Eq. (15) can be differentiated, obtaining the ensuing relation:

$$\mathbf{A}\delta\mathbf{l} = \mathbf{B}\delta\mathbf{x} \tag{16}$$

where the ith row of matrix $\mathbf{B}$ is the vector $2(Q_i - P_i)$, which can be written as $2(\mathbf{x} + \mathbf{c}_i)$, where $\mathbf{c}_i$ is a constant vector for the ith row. This means that the determinant of $\mathbf{B}$ is linear in the variables x, y, and z.

The parallel singularity locus is therefore a plane in the three-dimensional Euclidean space, because it is determined by the equation:

$$J_p = \det \mathbf{B} = 0 \tag{17}$$

which is linear in the variables x, y, and z.

Parallel singularities derived by Eq. (17) are not the only dangerous configurations for a 3UPU manipulator. Eq. (17) is based upon the implicit assumption that only translational virtual displacement of the platform are allowed, but there is no direct kinematic constraint enforcing this condition. Translational motion is the result of the particular choice of the U-joint axes, which might be unable to hinder virtual rotations at some singular positions.

These singular positions were named in (Zlatanov et al., 2002) *constraint singularities*, because at such positions some constraints of the parallel architecture are locally lost. Constraint singularities are typical of lower mobility parallel manipulators where the platform possesses less than six degrees of freedom. In such manipulators, some of the six degrees of freedom of the platform are controlled through the actuators of the manipulator, whereas some other (the rotational ones, in the case at hand) are passively constrained through the geometry of the legs. Parallel singularities are always detected by differentiating the equations connecting the input variables of the jointspace to the output variables of the workspace, but constraint singularities may not. In order to detect constraint singularities is always necessary to consider all six degrees of freedom of the platform, and to investigate under which conditions the constraints upon the degrees of freedom that are not controlled by the actuators might fail.

Constraint singularities of translational 3UPU manipulators were studied and rigorously determined in (Parenti Castelli & Di Gregorio, 2002). Constraint singularities are organized in a locus, which is defined by the ensuing equation:

$$J_c = \det \mathbf{C} = 0 \tag{18}$$

The ith column of the 3x3 matrix $\mathbf{C}$ is the axis direction of the rotation hindered by the ith leg, that can be expressed as follows:

$$t_i = \left(\mathbf{q}_i + \mathbf{x} - \mathbf{p}_i\right) - \left[\left(\mathbf{q}_i + \mathbf{x} - \mathbf{p}_i\right)^T \mathbf{r}_i\right]\mathbf{r}_i \tag{19}$$

Eq. (19) is a third order polynomial in the coordinates x, y and z, identifying the configuration of the manipulator.

Both constraints and parallel singularities are equally dangerous for a 3UPU translational manipulator, and must be avoided while moving from a configuration to another. The surface to be avoided is the zero level set of the function $J_p J_c$ on the workspace of the 3UPU translational manipulator. Unfortunately, the workspace of a translational manipulator is the three-dimensional Euclidean space, which is not compact. Thus, the method developed in Section 3 cannot be straightforwardly applied, because it works on compact manifolds only.

Yet, it is possible to transform the three-dimensional Euclidean space into a compact manifold. First of all, consider the three-dimensional real projective space associated to the three-dimensional Euclidean space, i.e. each vector (x_0, x_1, x_2, x_3) of the projective space is such that $(x, y, z) = (x_1 / x_0, x_2 / x_0, x_3 / x_0)$. Each point of the projective space corresponds to one point of the Euclidean space, except the points with $x_0 = 0$, i.e. points at infinity, that do not exist in the Euclidean space.

We can imagine the workspace of the 3UPU manipulator as the projective space, where the points with $x_0 = 0$ must never be crossed, exactly like singularities. Thus, the locus of "forbidden" points, is defined by the ensuing equation in the real projective space:

$$J = x_0 J_p J_c = 0 \tag{20}$$

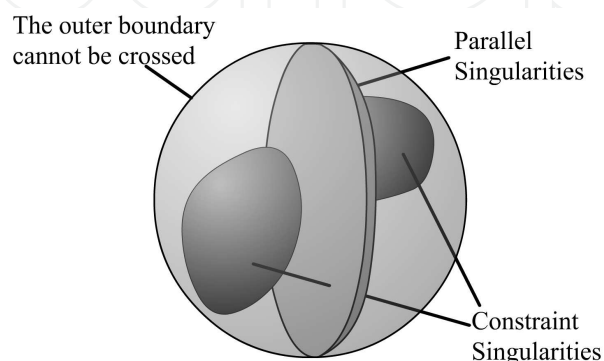where J_p and J_c are properly converted to homogeneous coordinates.

Fig. 9. Singularity locus of the 3UPU translational manipulator.

The real projective space can be represented as a ball, analogous to the manifold containing all orientations of a rigid body. With reference to Fig. 9, a three-dimensional ball with radius 1 is considered. For any point inside the ball, the coordinates of the point are the homogeneous coordinates x_1, x_2, and x_3, of the corresponding point in the projective space. The projective coordinate x_0 is defined as $x_0 = \sqrt{1 - x_1^2 - x_2^2 - x_3^2}$. In this way, all the points of the ball correspond to one point of the projective space. Furthermore, all points on the spherical boundary of the ball are points with $x_0 = 0$, i.e. points at infinity. Like Euler parameters, we represent a point of the projective space as a four-dimensional vector $\mathbf{x}_* = (x_0, x_1, x_2, x_3)$ with the constraint:

$$c = \mathbf{x}_*^T \mathbf{x}_* = 1 \tag{21}$$

The critical points of J on the configuration space must be found. The configuration space is the three-dimensional real projective space, and the critical points can be found through Lagrange multipliers method:

$$\frac{\partial J}{\partial \mathbf{x}_*} = \lambda \frac{\partial c}{\partial \mathbf{x}_*} \tag{22}$$

Lagrange multiplier λ can be easily eliminated considering the equation set:

$$\begin{aligned} T_1 &= (\partial J / \partial x_1) x_0 - (\partial J / \partial x_0) x_1 = 0 \\ T_2 &= (\partial J / \partial x_2) x_0 - (\partial J / \partial x_0) x_2 = 0 \\ T_3 &= (\partial J / \partial x_3) x_0 - (\partial J / \partial x_0) x_3 = 0 \end{aligned} \tag{23}$$

obtained by extracting λ from the first equation and then substituting it into the remaining three. Eq. (23) is a set of three homogeneous equations of degree five. Any critical point with $x_0 = 0$ must not be considered, because it lies on the locus $J = 0$. Thus $x_0 = 1$ can be substituted into Eq. (23), which is solved in terms of x_1, x_2, and x_3.

Since J is divisible by J_c and J_p, Eq. (23) can be written in the ensuing form:

$$\mathbf{M} \begin{pmatrix} J_c \\ J_p \\ J_c J_p \end{pmatrix} = \mathbf{0} \tag{24}$$

Therefore all points where $J_c = J_p = 0$ are critical points of J. These points form in general a curve in the workspace, and, not being isolated, are always degenerate critical points. Fortunately, the critical points where $J_c = J_p = 0$ are all singular, and must be ruled out of the analysis. Thus, only critical points where either J_c or J_p do not vanish must be considered, which, along with Eq. (24) yields the additional equation:

$$T_4 = \det \mathbf{M} = 0 \tag{25}$$

Eq.(25) is a third order equation in x_1, x_2, and x_3 and can be used to reduce the degree of

Eq. (23). Each of the three polynomials T_1, T_2, and T_3 can be written as follows:

$$T_i = T_4 Q_i + R_i \qquad (26)$$

where Q_i and R_i are the quotient and the remainder of a polynomial division on T_i through the divisor T_4 with respect to a given variable x_j. At every point where all T_i vanish along with T_4, all remainders R_i must vanish too. Therefore the equation set

$$R_1 = R_2 = R_3 = T_4 = 0 \qquad (27)$$

is always equivalent to Eq. (23), along with the condition $T_4 = 0$. If R_1, R_2, and R_3 are remainders of polynomial divisions with respect to variables x_2, x_1, and x_1, respectively, R_1, R_2, and R_3 are polynomials of degree four in the two variables x_2 and x_3. Therefore the equation set:

$$R_1 = R_2 = R_3 = 0 \qquad (28)$$

can be solved with a method similar to that used for spherical wrists. Variable x_1 can be hidden in the coefficients, and a partial homogenization with respect to x_2 and x_3 yields a set of three homogeneous equations in three unknowns of degree four. A resultant polynomial in x_1 can then be found through classical elimination methods.
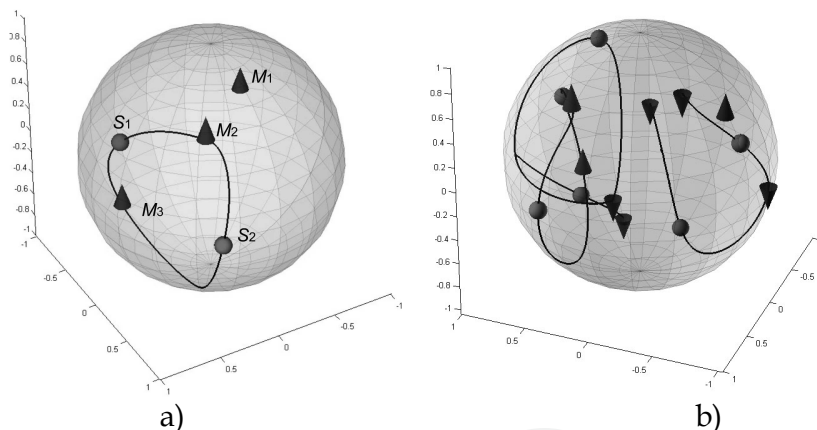

a)   b)

Fig. 10. a) Positive critical points of manipulator T_1;
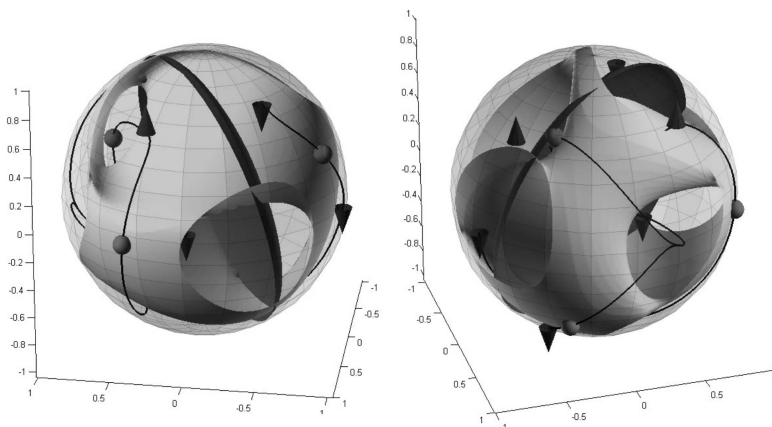b) All critical points of manipulator T_1.

Fig. 11. The steepest ascent and descent paths are all singularity-free.

Unfortunately, in this way the condition $T_4 = 0$ has not been directly imposed: Eq.(28) is not completely equivalent to Eq.(27), which introduces extraneous solutions. The author has found no way to factor out such extraneous solutions from the resultant polynomial, however they can be easily detected, for they do not satisfy the condition $T_4 = 0$.

Once all real solutions have been found by numerically solving the resultant polynomial, and all extraneous solutions have been cancelled, all critical points of J are known. The classification of critical points, and the determination of steepest ascent paths is then analogous to the one proposed in Section 4.1 for spherical wrists.

Manipulator T_1 is now considered as a numerical example. According to the conventional parameterization adopted before, T_1, is defined by vectors reported in Table 2.

$\mathbf{p}_1$	$\mathbf{p}_2$	$\mathbf{p}_3$	$\mathbf{q}_1$	$\mathbf{q}_2$	$\mathbf{q}_3$	$\mathbf{r}_1$	$\mathbf{r}_2$	$\mathbf{r}_3$
(1,0,0)	(0,1,0)	(0,1,-1)	(1,1,1)	(0,1,-1)	(1,1,1)	$(1,0,1)/\sqrt{2}$	$(1,0,1)/\sqrt{2}$	$(1,0,1)/\sqrt{2}$

Table 2. Parameters defining manipulator T_1

In the workspace of T_1 there are three positive maxima and two positive 2-saddles, shown in Fig. 10. a) Positive critical points of manipulator T1;Fig. 10a through the conventional ball visualization proposed in Fig. 9. Fig. 10a also shows the steepest ascent paths (black lines), departing from the positive 2-saddles and reaching the maxima. It can be seen that maxima M_2 and M_3 are joined, while no paths reach maximum M_1. Therefore there are two positive regions, free of parallel and constraint singularities.

There are five negative minima and four negative 1-saddles, and the network of steepest descent paths is such that there are also two negative regions.

Fig. 10b shows all relevant critical points: the positive maxima are depicted as upward bound cones, the negative minima as downward bound cones, and the saddle points as spheres. The network of singularity-free steepest ascent and descent paths is represented as black lines.

Fig. 11 shows two rotated views of the locus $J = 0$. The outer spherical boundary belongs to the locus, but it has not been plotted, in order for the inside of the ball to be visible. The darker surface inside the ball represents the locus of parallel singularities, whereas the brighter surface the locus of constraint singularities. The intersection curve of the two surfaces is a set of singular degenerate critical points, that have been ruled out from the determination of critical points by means of the polynomial division. It is possible to verify that the steepest ascent and descent paths never cross the spherical boundary, nor the parallel and constraint singularity loci.

4.3 3RRR Planar manipulators

A 3RRR planar manipulator with general structure is depicted in Fig. 12. The platform is connected to the rigid frame through three legs, composed of two connecting rods and three revolute joints, with the middle one actuated.

The center of the ith leg revolute joint on the fixed frame is indicated by P_i, whereas the center of the ith leg revolute joint on the platform is indicated by Q_i. The center of the actuated revolute joint of the ith leg is denoted by R_i.

The kinematic structure of the platform can be determined through the three parameters u_2, u_3, and v_3, defining the coordinates of Q_1, Q_2, and Q_3 in the reference frame uQ_1v attached to the platform, as shown in Fig. 12.. Analogously, the kinematic structure of the fixed frame is given by the three parameters a_2, a_3, and b_3, defining the coordinates of P_1, P_2, and P_3 in the fixed reference frame $xP_1 y$. The ith leg can be defined through the lengths of the two connecting rods: l_i and m_i (see Fig. 12). Thus twelve parameters are used to define a 3RRR manipulator.

This class of planar manipulators have been widely studied, and often used as an example, due to its simple kinematic architecture. Workspace analysis methods for similar manipulators were proposed in (Pennock & Kassner, 1993) and (Merlet et al.,1998) and the singularity locus of analogous manipulators was defined and studied in (Sefrioui & Gosselin, 1995) and (Wang & Gosselin, 1997).

The workspace of a 3RRR planar manipulator is a subset of the manifold containing all possible positions of the platform in the plane. Each point of the workspace will be identified by the coordinates x and y of point Q_1 in the fixed reference frame xP_1y and by the angle φ between x- and u-axes.
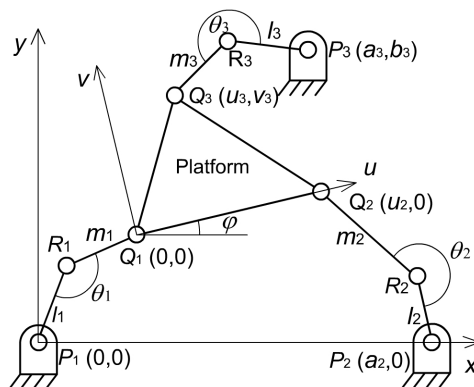

Fig. 12. A 3RRR manipulator.

The position of the ith actuator is given by the angle θ, between the two rods composing each leg. Any point in the jointspace is therefore identified by the three angles $(\theta_1, \theta_2, \theta_3)$.

Any configuration of the manipulator can be represented through the six parameters $(x, y, \varphi, \theta_1, \theta_2, \theta_3)$. However, not any combination of these six parameters identifies a configuration of the manipulator, for the ensuing constraints imposed by the three legs must be satisfied:

$$\mathbf{f} = \mathbf{0} \qquad (29)$$

where $f=(f_1, f_2, f_3)$, and

$$f_i = (P_i - Q_i(x, y, \varphi))^2 - l_i^2 - m_i^2 + 2m_i l_i \cos\theta_i, \qquad i = 1, 2, 3 \qquad (30)$$

Eq.(29) can be easily derived by expressing the coordinates of each Q_i in the fixed reference frame xP_1y, and by applying Carnot theorem to the three triangles $P_iQ_iR_i$.

The configuration space can be represented as the three dimensional manifold C described by Eq. (29) and embedded in the six dimensional manifold containing all the possible vectors $(x, y, \varphi, \theta_1, \theta_2, \theta_3)$.

Unlike the manipulators presented so far, the configuration space of planar 3RRR manipulators does not coincide with the workspace, and might be composed of more than one assembly configuration, therefore the proposed method will be applied to determine also the number of ACs and existence of feasible paths between any two configurations.

In order to derive the equation of the singularity locus the relationship between the first order displacements of the platform and the actuators is needed. Such relationship is obtained by differentiating Eq. (29):

$$\frac{\partial \mathbf{f}}{\partial \mathbf{s}} \delta \mathbf{s} + \frac{\partial \mathbf{f}}{\partial \mathbf{q}} \delta \mathbf{q} = \mathbf{0} \tag{31}$$

where $\mathbf{s}=(x, y, \varphi)$ and $\mathbf{q}=(\theta_1, \theta_2, \theta_3)$. Parallel singularities occur when the platform can undergo infinitesimal displacements $\delta \mathbf{s}$, even though all actuators are locked, i.e. $\delta \mathbf{q}$ vanishes. Thus all singular points must satisfy the condition:

$$J(x,y,\varphi) = \det\left(\frac{\partial \mathbf{f}}{\partial \mathbf{s}}\right) = 0 \tag{32}$$

The singularity locus is a two-dimensional manifold defined by the zero level-set of the function J, on the three-dimensional configuration space C.

Lagrange's optimization method is used again to find out critical points. The Lagrangian function L can be defined as:

$$L(x,y,\varphi,\theta_1,\theta_2,\theta_3,\lambda_1,\lambda_2,\lambda_3) = J - \lambda_1 f_1 - \lambda_2 f_2 - \lambda_3 f_3 \tag{33}$$

where f_1, f_2, and f_3, are defined by Eq.(30). The critical points of J constrained on C are the points where the gradient of L with respect to all its nine variables vanishes.

By equating to zero the derivatives of L with respect to the ith actuator angle θ_i, the ensuing equations are obtained:

$$\lambda_i \sin(\theta_i) = 0, \qquad i=1,2,3. \tag{34}$$

Therefore, the following four cases are given.

Case a): All Lagrange's multipliers λ_i are not equal to zero.
In this case the sine of the three angles θ_i must vanish (Eq.(34)), thus all three legs are completely outstretched or folded-up, for θ_i is equal to 0 or π. Such positions can be obtained by substituting all possible combinations of 0 and π into each θ_i of Eq.(29), which is reobtained as derivatives of L with respect to Lagrange's multipliers. By subtracting the first equation of Eq.(29) from the last two, two linear equations in x and y are obtained. From these linear equations, x and y can be determined as functions of the sine and cosine of φ, and back substituted into the first of Eq. (29), yielding a trigonometric equation in φ, which is easily solved through standard techniques. Lagrange's multipliers, which are useful for the classification of critical points, can be determined through the remaining derivatives of L.

Case b): ith Lagrange's multiplier is equal to zero.
In this case, only the sines of θ_j and θ_k vanish, with j and k different from i. Analogous to the previous case, two equations for x, y, and φ are obtained by substituting all possible

combinations of 0 and π into the cosine of θ_j and θ_k, in the jth and the kth equations of Eq. (29). By subtracting one of such equations from the other, a linear equation in x is obtained:

$$g(y,\varphi)x + h(y,\varphi) = 0 \qquad (35)$$

which yields x as a function of y and φ. By equating to zero the derivatives of L with respect to x, y, and φ, the ensuing equation is obtained:

$$\mathbf{A}(x,y,\varphi) \cdot (1, -\lambda_j, -\lambda_k)^T = \mathbf{0} \qquad (36)$$

where **A** is a 3×3 matrix, whose columns contain the gradients of J, f_j, and f_k with respect to variables x, y, and φ. Eq.(36) implies that the determinant of **A** must vanish, which yields the third condition in x, y, and φ. By substituting the expression of x obtained from Eq.(35) into this equation and into the jth equation of Eq.(29), the variable x is eliminated, and two polynomial equations in y and the tangent of $\varphi/2$ are obtained, which can be easily solved through Sylvester dyalitic elimination method (see Salmon, 1885). Among the solutions just obtained, there are some extraneous solutions, which can be easily got rid of, for at such solutions the two coefficients g and h of Eq.(35) vanish. The angles θ_j and θ_k are equal to 0 or π, whilst the angle θ_i can be derived from the ith equation of Eq. (29). The jth and kth Lagrange's multipliers are obtained from Eq. (36), and the ith is obviously zero.

Case c): ith and jth Lagrange's multipliers vanish.

By equating to zero the derivatives of L with respect to x, y, and φ, the ensuing equation is obtained:

$$\mathbf{B}(x,y,\varphi) \cdot (1, -\lambda_k)^T = \mathbf{0} \qquad (37)$$

Where B is a 3×2 matrix, whose columns contain the gradients of J and fk with respect to variables x, y, and φ. Eq.(37) implies that all the three 2×2 minors of B are singular, which yields three equations. By considering two of the three conditions just derived, along with the equation obtained by substituting 0 or π into θk in the kth equation of Eq. (29), three equations in the variables x, y, and φ are obtained, which can be solved analogously to case b). It is possible to prove that, by equating to zero only two of the three 2×2 minor determinants, some extraneous solutions are introduced, which do not make the third determinant vanish. By imposing this last condition, it is possible get rid of such extraneous solutions.

Case d): All Lagrange's multipliers are equal to zero.

In this case the gradient of J with respect to x, y, and φ must vanish, which yields two linear equations in x and y, and a quadratic equation in x and y. This equation set can be solved by techniques analogous to case a).

Once the critical points are determined, they are all classified by means of the bordered Hessian, as discussed in Section 4.1, and the maximum increase and decrease directions in the neighbourhoods of the saddle points are determined.

Two numerical examples are presented hereafter, manipulators P_1 and P_2. The kinematical structure of the two examples is summarized in Table 3, according to the parameterization adopted.

	a_2	a_3	b_3	u_2	u_3	v_3	l_1	m_1	l_2	m_2	l_3	m_3
P_1	10	3	10	10	3	3	1	2	10	2	6	7
P_2	10	3	10	10	3	3	1	2	4	2	5	6

Table 3. Parameters defining manipulators P_1 and P_2.

In manipulator P_1 there are four positive maxima, nine positive 2-saddles, four negative 2-saddles, and no negative maxima. The four positive maxima are shown in Fig. 13a. Maxima M_1 and M_2 are joined by steepest ascent paths starting from some of the positive 2-saddles, while M_3 and M_4 are not connected to any other maximum by any steepest ascent path starting from any positive or negative 2-saddle. There are three ACs: one containing M_1 and M_2, and the other two containing M_3 and M_4. Manipulator P_1 was generated by imposing that the loop composed by leg 1, leg 2, the platform and the frame have two ACs, through the condition derived in (Foster & Cipra, 1998), and that leg 3 be able to completely outstretch in one of such ACs, but not in the other. Therefore one of the two ACs of the loop is split into two ACs by the fact that leg 3 can never outstretch, nor fold back.
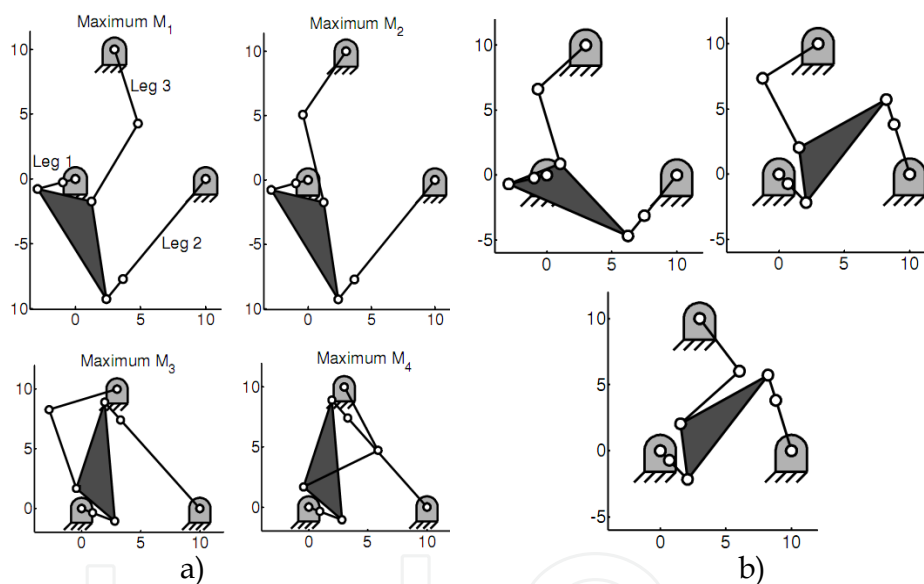

Fig. 13. a) The four maxima of manipulator P_1.
b) Three maxima of manipulator P_2.

The analysis of the negative critical points shows that each of the tree ACs is split into two PSFRs, one positive, and one negative. Therefore, if the sign of the Jacobian determinant is the same at two configurations belonging to the same AC, a singularity-free path connecting them always exists.

However, the ACs are not always split into two PSFRs only, as manipulator P_2 shows. In manipulator P_2 there is only one AC, therefore any configuration of the manipulator is reachable, but this AC is split into four PSFRs, three positive and one negative. Fig. 12b shows three positive maxima belonging to the three positive PSFRs: many feasible paths connect these three configurations where the Jacobian determinant is positive, but none of them is free of parallel singularities.

7. Conclusion

This work presented a numerical method able to count and identify the PSFRs and the ACs carved by the singularity locus in the configuration space of a manipulator, and its application to three types of parallel manipulators.

In principle, this method works for any manipulator, but some very particular cases, where there are degenerate critical points of the Jacobian determinant. The application is rather simple, except the determination of all critical points of the Jacobian determinant on the configuration space. This part of the procedure reduces in most cases to the determination of all solutions to a polynomial equation set, that might be a very hard task in practice, although it is always theoretically possible.

However, if the determination of the critical points of the Jacobian determinant is viable, like the presented examples, the proposed method represents a stable and powerful tool for analyzing the topology of the singularity locus and for planning singularity-free paths.

The proposed method does not take into account the possible reduction of configuration space of a manipulator due to the mechanical interference between the links, or by actuator limits. The analysis of the singularity locus under the additional constraint that no collision between the links takes place is a possible future development of the proposed method, as well as its application to more parallel manipulators with six degrees of freedom.

8. References

Bhattacharya, S., Hatwal, H., and Ghosh, A., 1998, "Comparison of an exact and an approximate method of singularity avoidance in platform type parallel manipulators," Mechanism and Machines Theory, 33(7), pp. 965–974.

Chablat, D. and Wenger, P., 1998, "Working modes and aspects in fully parallel Leuven, Belgium, pp. 1964–1969.

Chase, T.R. and Mirth, J.A., 1993, "Circuits and branches of single-degree-of-freedom planar linkages," Journal of Mechanical Design, 115(2), pp. 223-230.

Dasgupta, B. and Mruthyunjaya, T., 1998, "Singularity-free path planning for the Stewart platform manipulator," Mechanism and Machine Theory, 33(6), pp. 711–725.

Di Gregorio, R., and Parenti-Castelli, V., 1998, "A Translational 3-dof Parallel Manipulator," Advances in Robot Kinematics: Analysis and Control Lenarcic, J., and Husty, M. L., Eds., Kluwer Academic Publishers, pp. 49-58.

Di Gregorio, R., and Parenti Castelli V., 2002, "Mobility Analysis of the 3-UPU Parallel Mechanism Assembled for a Pure Translational Motion," Journal of mechanical Design,Vol. 124, pp. 259-264.

Dou, X. and Ting, K.L., 1998, "Identification of singularity free joint rotation space of two-dof parallel manipulators," proceedings of DETC'98, Atlanta, Georgia.

Fletcher, R.,1987, Practical Methods of Optimization, John Wiley & Sons, Chichester.

Foster, D.E. and Cipra, R.J., 1998, "Assembly configurations and branches of single-loop mechanism with pin joints and sliding joints," Journal of Mechanical Design, 120(3), pp. 387-391.

Foster, D.E. and Cipra, R.J., 2002, "An automatic method for finding the assembly configurations of planar non-single-input-dyadic mechanisms," Journal of Mechanical Design, 124(1), pp. 58-67.

Gosselin, C. and Angeles, J., 1990, "Singularity analysis of closed-loop kinematic chains," IEEE Transactions On Robotics and Automation, 6(3), pp. 281–290.

Hirsch, M.W., 1976, Differential Topology, Springer, New York.

Innocenti, C., and Parenti-Castelli, V. , 1993, "Echelon form solution of direct Kinematics for the general fully-parallel spherical wrist," Mechanism and Machine Theory, vol. 28, No.4, pp. 553–561.

Kevin Jui C.K. and Qiao Sun, 2005, "Path tracking of parallel manipulators in the presence of force singularity," Journal of Dynamic Systems, Measurement and Control, 127, pp. 550–563.

Merlet, J.P., Gosselin, C.M., and Mouly, N., 1998, "Workspaces of planar parallel manipulators," Mechanism and Machine Theory, 33(1/2), pp.7-20.

Milnor, J., 1969, Morse Theory, Princeton University Press.

Mirth, J.A. and Chase, T.R., 1993, "Circuit analysis of Watt chain six-bar mechanisms," Journal of Mechanical Design, 115(2), pp.214-222.

Midha, A., Zhao, Z.L., and Her, I., 1985, "Mobility conditions for planar linkages using triangle inequality and graphical interpretation," Journal of Mechanical Design, 107(3), pp. 394-400.

Paganelli, D., 2008, "Topological Analysis of Singularity Loci for Serial and Parallel Manipulators,"Phd. Thesis, University of Bologna.

Paul, B., 1979, "A reassessment of Grashof's Criterion," Journal of Mechanical Design, 101, pp. 515-518.

Parenti-Castelli, V., Di Gregorio, R., and Lenarcic, J., 1998, "Sensitivity to Geometric Parameter Variation of a 3-dof Fully-Parallel Manipulator," Proceedings of the 3rd International Conference on Advanced Mechatronics, pp. 364-369.

Pennock, G.R. and Kassner, D.J., 1993, "The workspace of a general geometry planar three-degree-of-freedom platform-type manipulator," Journal of Mechanical Design, 115(1), pp. 269-276.

Salmon, G. , 1885, Modern Higher Algebra, Hodges, Figgis & Co., Dublin.

Sen, S. , Dasgupta, B., and Mallik, A.K., 2003, "Variational approach for singularity-free path-planning of parallel manipulators," Mechanism and Machine Theory, 38, pp. 1165–1183.

Sefrioui, J., Gosselin, C., 1994, "Etude et Representation des Lieux de Singularite des Manipulateurs Paralleles Spheriques a Trois Degres de Liberte avec Actionneurs Prismatiques," Mechanisms and Machines Theory, 29, No.4, pp.559-579.

Sefrioui, J. and Gosselin, C.M., 1995, "On the quadratic nature of the singularity curves of planar three-degree-of freedom parallel manipulators," Mechanism and Machine Theory, 30(4), pp.533-551.

Tsai, L. W., 1996, "Kinematics of a Three-dof Platform With Three Extensible Limbs," Recent Advances in Robot Kinematics, Lenarcic, J., and Parenti-Castelli, V., Eds., Kluwer Academic Publishers,pp. 401-410.

Wang, J., and Gosselin, C.M., 1997, "Singularity loci of planar parallel manipulators with revolute actuators," Robotics and Autonomous Sustems, 21, pp.377-398.

Whitehead, W., 1978, Elements of Homotopy Theory, Springer, New York.

Zlatanov, D., Bonev I.A., and Gosselin, C.N., 2002, "Constraint Singularities of Parallel Mechanisms," Proceedings of the 2002 IEEE International Conference on Robotics & Automation, pp. 496-502.

Robot Manipulators Trends and Development

Edited by Agustin Jimenez and Basil M Al Hadithi

This book presents the most recent research advances in robot manipulators. It offers a complete survey to the kinematic and dynamic modelling, simulation, computer vision, software engineering, optimization and design of control algorithms applied for robotic systems. It is devoted for a large scale of applications, such as manufacturing, manipulation, medicine and automation. Several control methods are included such as optimal, adaptive, robust, force, fuzzy and neural network control strategies. The trajectory planning is discussed in details for point-to-point and path motions control. The results in obtained in this book are expected to be of great interest for researchers, engineers, scientists and students, in engineering studies and industrial sectors related to robot modelling, design, control, and application. The book also details theoretical, mathematical and practical requirements for mathematicians and control engineers. It surveys recent techniques in modelling, computer simulation and implementation of advanced and intelligent controllers.

How to reference

In order to correctly reference this scholarly work, feel free to copy and paste the following:

INTECH

open science | open minds